

Effects of urolithin A on osteoclast differentiation induced by receptor activator of nuclear factor- κ B ligand via bone morphogenic protein 2

Zhe Wang^{a,b,#}, Guobin Qi^{a,#}, Zhuokai Li^c, Xu Cui^c, Shengyang Guo^c, Yueqi Zhang^a, Pan Cai^c, and Xiuhui Wang^c

^aDepartment of Orthopedics, Zhongshan Hospital, Fudan University, Shanghai, China; ^bDepartment of Orthopedic Surgery, School of Medicine, Johns Hopkins University, Baltimore, MD, USA; ^cDepartment of Orthopedics, Shanghai University of Medicine & Health Sciences Affiliated Zhoupu Hospital, Shanghai, China

ABSTRACT

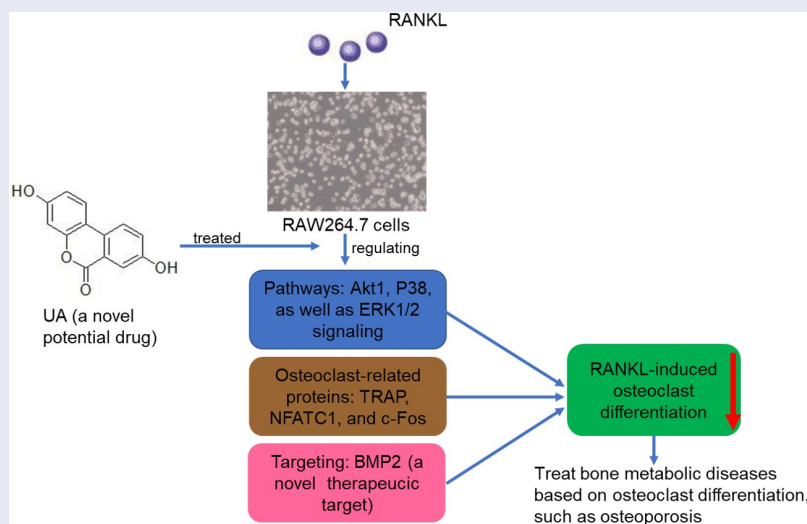
Urolithin A (UA) is an intestinal microbial metabolite derived from ellagitannins and a promising agent for treating osteoarthritis. However, its effects on osteoporosis are unclear. This study explored the effects of urolithin A (UA) on receptor activator of nuclear factor- κ B ligand (RANKL)-induced osteoclasts and its underlying molecular mechanisms. RANKL treatment significantly increased tartrate-resistant acid phosphatase (TRACP) or osteoclast marker levels ($P < 0.05$), while adding UA decreased the RANKL-induced levels ($P < 0.05$) in RAW264.7 cells. Total RNA isolated from RANKL- or RANKL + UA-treated cells was sequenced, and the obtained transcriptome dataset revealed 2,399 differentially expressed genes. They were enriched in multiple pathways involved in rheumatoid arthritis, ERK1 and ERK2 cascade, regulation of inflammatory response, ECM-receptor interactions, and TNF signaling. Scanning electron microscopy showed that RANKL promoted bone resorption pits in bone biopsy specimens, whereas UA inhibited their formation. When bone morphogenic protein 2 (BMP2) was *shRNA*-silenced, the bone resorption pits were restored. Moreover, while RANKL significantly enhanced the levels of p-ERK2/ERK2, p-p38/p38, p-Akt1/Akt1, p-ERK1/ERK1, and osteoclast-related proteins ($P < 0.05$), UA reduced them. BMP2 silencing also reversed the UA inhibitory effect. Thus, UA represses the RANKL-induced osteoclast differentiation of RAW264.7 cells by regulating Akt1, p38, and ERK1/2 signaling, and BMP2 likely reverses the UA inhibitory effect via these pathways. We propose BMP2 as a potential drug target for treating bone metabolic diseases, such as osteoporosis.

ARTICLE HISTORY

Received 20 December 2021
Revised 27 January 2022
Accepted 28 January 2022

KEYWORDS

RAW264.7 cells; osteoclast; urolithin A; RANKL; BMP2; transcriptome sequencing



Background

Bone remodeling involves the dynamic coupling of osteoblast bone formation and osteoclast bone resorption[1]. Under normal conditions, osteoblasts and osteoclasts coordinate to establish homeostasis between the two processes, maintaining normal bone function[2]. Under disease conditions, such as rheumatoid arthritis, osteoporosis, and lytic bone metastases, excessive bone resorption causes imbalance leading to bone loss[3]. Osteoporosis is a life-threatening medical problem that increases with prolonged human life expectancy [4,5]. It often leads to fractures and other complications, such as pro-lapse pneumonia, deep vein thrombosis, and bedsores, which can be fatal[6]. Currently, the main agents used to treat osteoporosis are anti-resorptive (e.g., bisphosphonates, denosumab, and calcitonin) and anabolic (strontium ranelate)[7]. However, their efficacy is unsatisfactory and long-term use can lead to numerous adverse effects. Therefore, discovering new therapeutic strategies to manage osteoporosis is critical.

Urolithin A (UA) is an intestinal microbial metabolite of ellagic acid and ellagitannins. It has high bioavailability and multiple health benefits, including anti-inflammatory and anti-proliferative effects against cancer, antioxidant activity, and improved lipid metabolism [8,9]. A first-in-human clinical trial demonstrated that UA is safe and can induce molecular signatures of improved mitochondrial and cellular health following regular oral consumption[10]. Additionally, UA attenuates the inflammatory response and cartilage degradation induced by IL-1 β by inhibiting mitogen-activated protein kinase (MAPK)/ nuclear factor kappa B subunit 1NF- κ B signaling pathways. Thus, UA is a promising agent for treating osteoarthritis (OA)[11]. Lin et al.[12] indicated that UA promotes mitophagy by protein kinase AMP-activated catalytic subunit alpha 1 (AMPK) signaling activation in tert-butyl hydroperoxide-treated nucleus pulposus cells, inhibiting the treatment-induced mitochondrial dysfunction and apoptosis. It also alleviates the progression of puncture-induced intervertebral disc degeneration in vivo. However, UA effects on osteoporosis and

its underlying molecular mechanisms remain unclear.

Osteoclasts are key participants in bone resorption and unique multinuclear cells originating from the mononuclear/macrophage lineage of the bone marrow[13]. Therefore, they may be the targets for osteoporosis treatment [14]. Their differentiation and function are regulated by various systemic hormones, cytokines, and the central osteoclastogenic molecule called receptor activator of nuclear factor- κ B ligand (RANKL)[13]. The interaction between RANKL and its receptor (RANK) activates several transcription factors and signaling pathways[15], stimulating the expression of genes that control osteoclast differentiation and functions and promoting osteoclast formation and maturation[16]. Excessive osteoclast activity in osteoporosis causes an imbalance in bone remodeling; therefore, inhibiting it is essential in preventing and treating osteoporosis.

RAW264.7 is a mature pre-osteoclast cell line that can differentiate into osteoclasts after induction by specific growth factors, such as RANKL [17]. RANKL, expressed as a membrane-associated cytokine, has been used to induce osteoclastic differentiation in the RAW264.7 cells[1], as well as RANKL-treated RAW264.7 cells are often used to study osteoclast genesis in vitro. Therefore, in our study, RANKL was used to induce osteoclast differentiation of RAW264.7 cells and UA to treat the differentiated cells. Effects of UA on osteoclast activity were evaluated, and its mechanisms were determined by transcriptome sequencing. The transcriptome analysis showed that bone morphogenic protein 2 (BMP2) mRNA levels were significantly affected by the UA treatment of the differentiated cells. To our knowledge, the members of the BMP family are key mediators of morphogenesis and differentiation in multiple tissues and play important roles in skeletal development[16]. Moreover, BMP2 regulates osteoclasts and osteoblasts and directly promotes RANKL-induced osteoclast differentiation [17,18]. Therefore, BMP2 was further investigated to determine its role in the UA-promoted inhibition of osteoclast formation. Our work

suggests a novel drug target for the treatment of osteoporosis.

Materials and methods

Cell culture

RAW264.7 cells, a kind of the mouse macrophage cell line, were purchased from the Cell Bank of Type Culture Collection of Chinese Academy of Sciences (Shanghai, China). The cells were cultured in high-glucose Dulbecco's Modified Eagle Medium (Thermo Fisher Scientific, Waltham, MA, USA) supplemented with 10% fetal bovine serum (Thermo Fisher Scientific) and 100 U/mL penicillin–100 µg/mL streptomycin (Thermo Fisher Scientific). The cells were maintained in a humidified incubator containing 5% CO₂ at 37°C.

Determination of optimal UA concentration

A Cell Counting Kit-8 (CCK-8; Beyotime Biotechnology, Beijing, China) was used to assess the optimal concentration of UA for treating RAW264.7 cells before subjecting them to RANKL-stimulated differentiation. The cells were seeded into 96-well plates at a density of 1×10^4 cells/well and cultured. The adhered cells were treated with 0, 0.5, 5, 25, 50, or 100 µM UA (Selleck Chemicals, Houston, TX, USA) and cultured at 37°C for 12, 24, 48, 72, and 96 h. Upon culturing, 10 µL of the CCK-8 reagent was added to each well, and the cells were incubated for another 2 h. The optical density (OD) was measured at 450 nm using a microplate reader (Thermo Fisher Scientific).

Quantification of tartrate-resistant acid phosphatase (TRACP)

RAW264.7 cells were divided into three treatment groups: control, RANKL, and RANKL + UA groups. Cells in the RANKL and RANKL + UA groups were treated with 100 ng/mL RANKL[18] and 100 ng/mL RANKL + 25 µM UA, respectively. Following 48 h of culturing, cells were lysed using cell lysis buffer (Beyotime Biotechnology), and the lysate was used for TRACP detection using

a TRACP content detection kit (Beyotime Biotechnology), according to the manufacturer's protocol. Briefly, 40 µL of the cell lysate was incubated at 37°C for 10 min, and 160 µL of stop solution was added. A microplate reader was used to measure the OD at 405 nm.

Transcriptome sequencing and analysis

The RNA samples isolated from the RANKL- and RANKL + UA-treated cells were sequenced at Yanzai Biotechnology Co, Ltd (Shanghai, China) on an Illumina (San Diego, CA, USA) sequencing platform. Clean data were obtained by removing low-quality sequences and adapter contamination. The HISAT2 software (<https://ccb.jhu.edu/software/hisat2/index.shtml>) was used for mapping, and gene expression levels were determined using the featureCounts software. The DESeq2 algorithm was used to identify differentially expressed genes (DEGs) based on the fold change (FC) cutoff of > 1.5 and false discovery rate (FDR) < 0.05. The DEGs were subjected to gene ontology (GO) and Kyoto Encyclopedia of Genes and Genomes (KEGG) functional analyses. The GO terms and KEGG pathways were considered significantly enriched if $P < 0.05$.

Acquisition of lentivirus packaging

Using the sequence reported by Fujimoto et al.[19] (GATCCGGGACACCAGGTTAGTGAATTTCAAGAGAATTCACCTAACCTGGTGTCCCTTTTTTCTCGAGG), a *BMP2* short hairpin RNA (shRNA) was synthesized by Yanzai Biotechnology Co, Ltd. The pGreenPuro vector was used to construct the *BMP2* shRNA vector, as previously described[20]. RAW264.7 cells were infected with 50 µL of the packaged *BMP2* shRNA vector suspension and cultured for 48 h. After 48 h, the complete medium containing 2 µg/mL puromycin was added to select for stable, transfected sh*BMP2*-RAW264.7 cells[21]. The stably transfected cells were expanded in culture for subsequent experiments. The *BMP2* primer sequences are shown in Table 1. Reverse transcription-quantitative PCR (RT-qPCR) evaluated the transfection efficiency by determining the *BMP2* expression.

Table 1. The sequences of all primers.

Gene	Sequence (5'-3')
TRAP	F: CACTCCCACCTGAGATTTGT R: CCCAGAGACATGATGAAGTCA
NFATC1	F: GGAGAGTCCGAGAATCGAGAT R: TTGCAGCTAGGAAGTACGCTT
c-Fos	F: CGGGTTTCAACGCCGACTA R: TGGCACTAGAGACGGACAGAT
BMP2	F: GGGACCCGCTGCTTCTAGT R: TCAACTCAAATTCGCTGAGGAC
Cebpa	F: CAAGAACAGCAACGAGTACCG R: GTCACCTGGTCAACTCCAGCAC
Clec4a3	F: CTCACCTCAACTGACTTGGTGG R: TCACTGCTAGGCTCACCTTTG
Mapk1ip1	F: CCCTCCAGCTAGACTACTACCA R: TGGAAAGGGCACATTTGTTGAAA
MMP3	F: ACATGGAGACTTTGTCCTTTTG R: TTGGCTGAGTGGTAGAGTCCC
MMP9	F: GCAGAGGCATACTTGTACCG R: TGATGTTATGATGGTCCCACTTG
RUNX2	F: ATGCTTCATTGCGCTCACAAA R: GCACTCACTGACTCGGTTGG
RUNX3	F: CAGGTTCAACGACCTTCGATT R: GTGGTAGGTAGCCACTTGGG
GAPDH	F: GGTGAAGGTCCGTTGTGAACG R: CTCGCTCCTGGAAGATGGT

RT-qPCR

Total RNA was extracted from RAW264.7 or shBMP2-RAW264.7 cells after the different chemical treatments using RNAiso Plus (Takara). The RNA quality and concentration were assessed using the 260/280 OD ratio. The isolated RNA with a high 260/280 ratio was reverse-transcribed into cDNA using PrimeScript RT Master Mix (Takara) and used as the template for RT-qPCR. The PCR assays were performed using SYBR Premix Ex Taq II (Tli RNaseH Plus, Takara) in an ABI 7500 detection system (Applied Biosystems, Foster City, CA, USA). The qPCR cycling conditions were as follows: 50°C, 2 min; 95°C, 2 min; 40 cycles at 95°C, 15s; 40 cycles at 60°C, 60s. All primer sequences are listed in Table 1. Glyceraldehyde-3-phosphate dehydrogenase (*GAPDH*) was used as a housekeeping gene, and the relative mRNA expression levels were calculated using the $2^{-\Delta\Delta Ct}$ method[22].

Scanning electron microscopy

Bone biopsies (IDS Imaging Development Systems Inc, Obersulm, Germany) were washed with medium and placed in 96-well plates. shNC-RAW264.7 cells (negative control) or shBMP2-RAW264.7 cells

were seeded into the wells containing the biopsies. The biopsies with shNC-RAW264.7 or shBMP2-RAW264.7 cells were treated with 100 ng/mL RANKL or 100 ng/mL RANKL and 25 μ M UA. Subsequently, the treated biopsy specimens were harvested and fixed with 2.5% glutaraldehyde. The images of the bone biopsies were obtained using a scanning electron microscope (Hitachi, Chiyoda City, Japan) and quantified using the NIH ImageJ software (Bethesda, MD, USA).

Western blotting

Total protein was isolated from RAW264.7 or shBMP2-RAW264.7 cells subjected to different treatments using radioimmunoprecipitation assay lysis buffer (Beyotime Biotechnology). Protein concentrations were determined using a bicinchoninic acid assay kit (Beyotime Biotechnology). The protein samples (20 μ g) were separated on a 10% sodium dodecyl sulfate-polyacrylamide gel, transferred to polyvinylidene fluoride membranes, and blocked with 5% skim milk at 37°C for 2 h. After washing with PBST (1 mL of Tween-20 in 1,000 mL of PBS) three times, the membranes were incubated with anti-Akt1 (1:1,000; Cell Signaling Technology, Danvers, MA, USA), anti-phosphorylated (p)-Akt1 (1:1,000; Cell Signaling Technology), anti-P38 (1:1,000; Cell Signaling Technology), anti-p-P38 (1:1,000; Cell Signaling Technology), anti-ERK (1:1000; Cell Signaling Technology), anti-phospho-ERK (1:1,000; Cell Signaling Technology), anti-RANK (1:1,000; Abcam, Cambridge, UK), anti-cathepsin K (1:1,000; Proteintech, Rosemont, IL, USA), anti-integrin β 3 (1:1,000; Abcam), or anti-GAPDH (1:1,000, Proteintech) antibodies at 4°C overnight. After washing with PBST three times, the membranes were incubated with the secondary antibody (1:5,000; Jackson ImmunoResearch Laboratories Inc, West Grove, PA, USA) at 37°C for 2 h. After washing the membranes with PBST five times, they were subject to an enhanced chemiluminescence assay (Beyotime Biotechnology). The protein bands were detected in a chemiluminescence imaging apparatus (Shanghai Tanon Science & Technology Co Ltd, Shanghai, China).

Statistical analysis

Data are reported as the mean \pm standard deviation. GraphPad Prism 5 (GraphPad Prism Software, San Diego, CA, USA) was used for statistical analyses. A Student's *t*-test was used to compare two groups, and a one-way analysis of variance to compare more than two groups. $P < 0.05$ was considered statistically significant.

Results

Determination of optimal UA concentration

RAW264.7 cells were treated with different concentrations of UA to determine the optimal concentration of UA, and the cytotoxic effects were determined using a CCK-8 assay. After 12 h in culture, no significant differences in the cell viability on different concentrations of UA were found ($P > 0.05$, Figure 1(a)). After 24 h or 48 h in culture, the viability of cells treated with 0, 0.5, 5, and 25 μM UA showed no significant difference compared with untreated cells ($P > 0.05$). The viability dropped only on 50 and 100 μM UA ($P < 0.05$, Figure 1(b,c)). After 72 h or 96 h, the viability of cells treated with 0, 0.5, and 5 μM UA

was unaffected ($P > 0.05$) but lower than the viability of untreated cells after 25, 50, and 100 μM UA ($P < 0.05$, Figure 1(d,e)). These results suggest that 25 μM UA and 48 h are optimal treatment conditions for RAW264.7 cells in subsequent experiments.

Effects of UA on osteoclast formation from RAW264.7 cells

TRACP was quantified to investigate UA effects on osteoclast formation from RANKL-treated RAW264.7 cells. The RANKL-treated cells had significantly higher TRACP levels than the control cells (Figure 2, $P < 0.05$). When RANKL-induced cells were UA-treated, their TRACP levels dropped to those similar in the control cells ($P > 0.05$, Figure 2(a)). Next, osteoclast-specific markers *NFATC1*, *c-Fos*, and *TRAP* were determined by RT-qPCR. The mRNA expression of all three markers was significantly increased in RANKL-treated cells versus the control cells ($P < 0.05$). By contrast, it was markedly decreased in UA-treated RANKL-induced cells ($P < 0.05$) and similar to that of control cells ($P > 0.05$, Figure 2(b-d)). These results indicate that 100 ng/mL RANKL

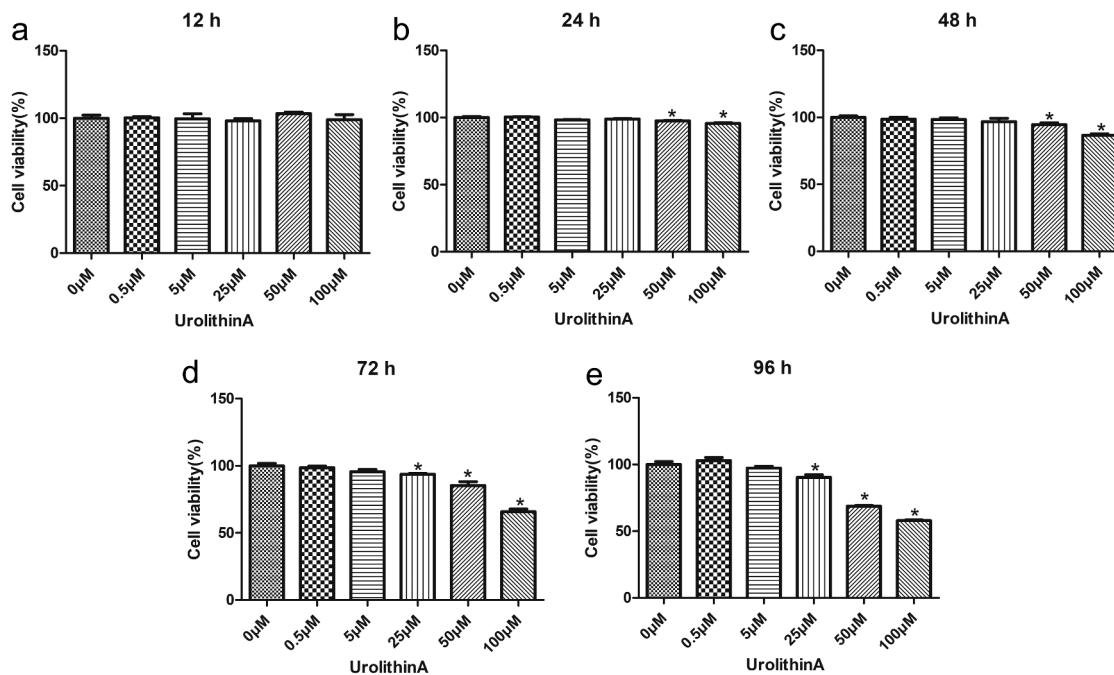


Figure 1. Determination of optimal urolithin A concentration for cell treatments. The viability of RAW264.7 cells treated with different concentrations of urolithin A (UA) for 12 h (a), 24 h (b), 48 h (c), 72 h (d), and 96 h (e) is compared with the viability of untreated cells (* $P < 0.05$). The cell viability was determined by a cell counting kit-8 assay.

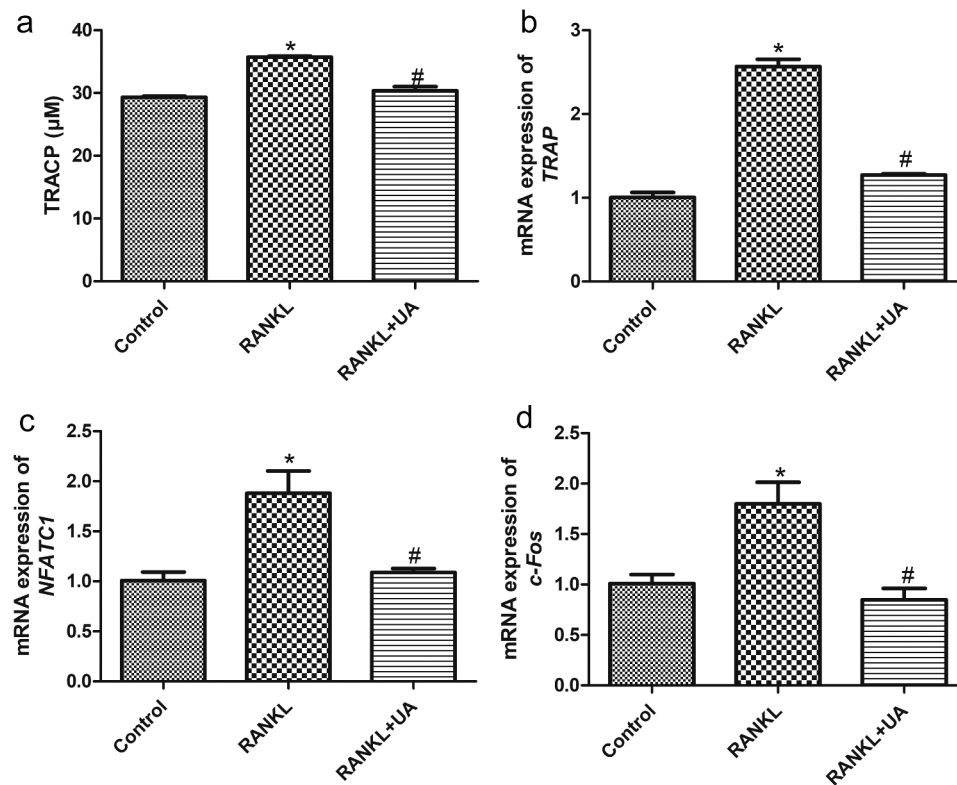


Figure 2. Urolithin A effects on osteoclasts differentiated from RANKL-treated RAW264.7 cells. (a) Tartrate-resistant acid phosphatase (TRACP) levels in RAW264.7 cells subject to RANKL or UA treatment. mRNA expression levels of (b) *TRAP*, (c) *NFATC1*, and (d) *c-Fos* in RAW264.7 cells subject to RANKL or UA treatment. * $P < 0.05$ represents significance compared with the control group, and # $P < 0.05$, compared with the RANKL-treated group.

successfully induced the osteoclast formation from RAW264.7 cells, and 25 μM UA inhibited the RANKL-induced osteoclast formation.

Identification and functional annotation analyses of DEGs

Total RNA samples isolated from RAW264.7 cells treated with RANKL or RANKL + UA were sequenced to explore the underlying molecular mechanisms of UA on osteoclast differentiation. Based on the Pearson's correlation analysis of each sample, we found no differences among the samples isolated from either the RANKL-treated cell group or the RANKL + UA-treated group. Conversely, we identified a significant difference between the samples from cells in the two different treatment groups (Figure 3(a)). According to the thresholds ($\text{FC} > 1.5$; $\text{FDR} < 0.05$), 2,399 DEGs were identified, of which 587 were upregulated and 1,812 downregulated (Figure 3(b)). Hierarchical clustering analysis of the identified DEGs distinguished cells in the RANKL-treated

group from those in the RANKL + UA-treated group, confirming the reliability of the above results (Figure 3(c)).

The DEGs were subjected to functional annotation analyses to assess their biological identity. Figure 4 shows the most enriched GO terms belonging to biological process (BP), cellular component (CC), and molecular function (MF) terms. The DEGs associated with the BP term were implicated in response to wounding, regulation of the ERK1/2 cascade, wound healing, and regulation of the inflammatory response. Those associated with the CC term were involved in extracellular matrix, adherens junction, and microtubule functions. The DEGs associated with the MF term were involved in sulfur compound binding, glycosaminoglycan binding, actin binding, and cell adhesion molecule binding (Figure 4(a-c)). In addition, KEGG analysis found that the DEGs were significantly enriched in rheumatoid arthritis, TNF signaling pathway, fluid shear stress, atherosclerosis, and ECM-receptor interactions (Figure 4(d)).

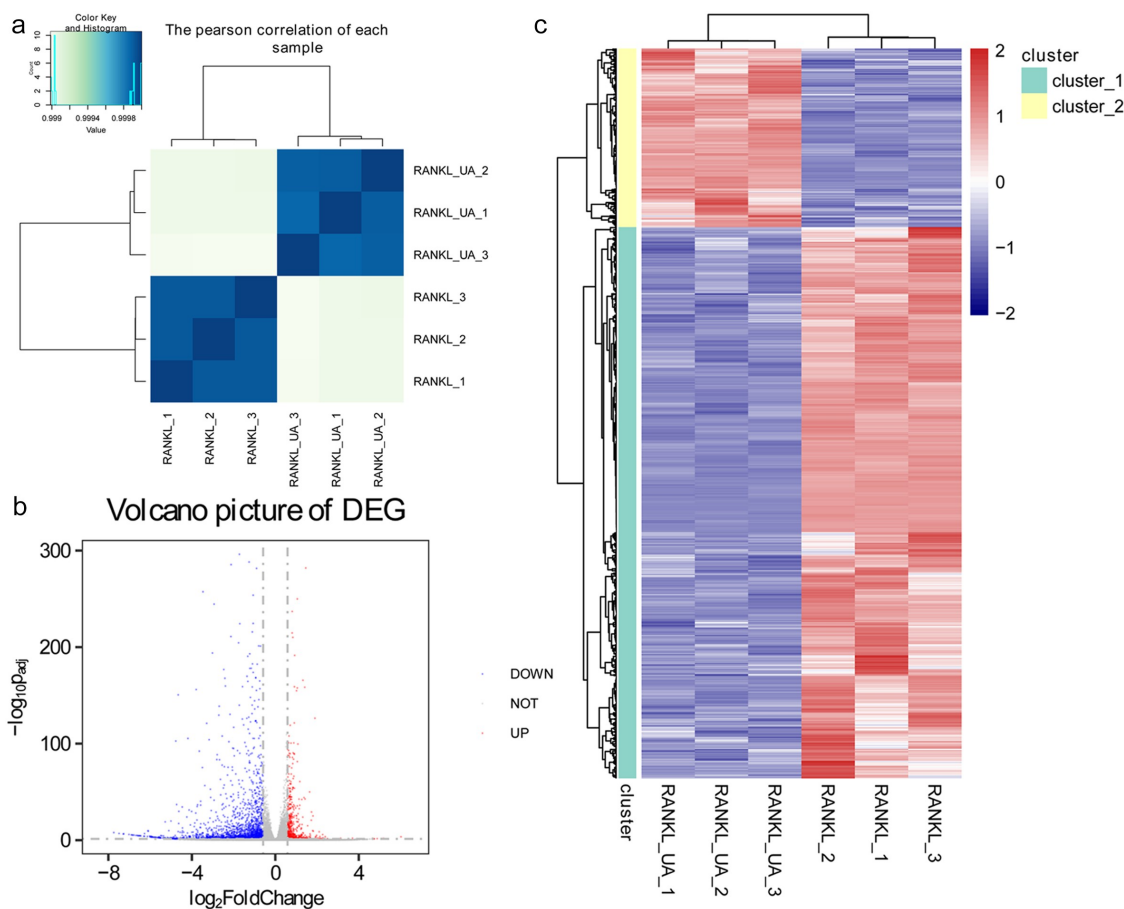


Figure 3. Identifying differentially expressed genes in RAW264.7 cells treated with RANKL or RANKL and UA. (a) Pearson's correlation coefficients for each total RNA sample isolated from RANKL- or RANKL + UA-treated cell group. (b) A volcano plot of the differentially expressed genes (DEGs). The blue points represent downregulated genes, the gray points normal expression levels, and the red points upregulated genes. (c) Clustering heatmap based on the expression level of the identified DEGs.

Verifying translome data by RT-qPCR

Four activated (*BMP2*, *Cebpa*, *Clec4a3*, and *Mapk1ip1*) and four repressed (*MMP3*, *MMP9*, *RUNX2*, and *RUNX3*) DEGs were quantified by RT-qPCR to validate the sequencing data. The expression levels of *BMP2*, *Cebpa*, and *Mapk1ip1* were significantly increased in RANKL + UA-treated cells compared with those in RANKL-treated cells ($P < 0.05$, Figure 5(a,b,d)). By contrast, the expression levels of *MMP3*, *MMP9*, and *RUNX2* were markedly decreased in these cells compared with those treated only with RANKL ($P < 0.05$, Figure 5(e-g)). These results are thus consistent with the expression pattern observed in the sequencing data. However, no significant differences were observed in *Clec4a3* and *RUNX3* expression between treated cells ($P > 0.05$, Figure 5(c,h)). Collectively, these findings imply

that the consistency rate between the RT-qPCR and sequencing analysis is 75%, which indicates a relatively high reliability of the sequencing data [23,24]. Furthermore, Western blotting showed that *BMP2* was significantly upregulated in the RANKL-induced cells ($P < 0.05$) versus the control cells. Moreover, UA further increased *BMP2* expression in the RANKL-treated cells (Figure 5(i)). Therefore, the role of *BMP2* in osteoclast differentiation was further investigated.

Cell transfection efficiency and scanning electron microscopy analysis

A *BMP2*-specific shRNA was used to silence *BMP2* in RAW264.7 cells to delineate *BMP2* effects on osteoclast formation. The relative expression of *BMP2* was considerably lower in the shNC-

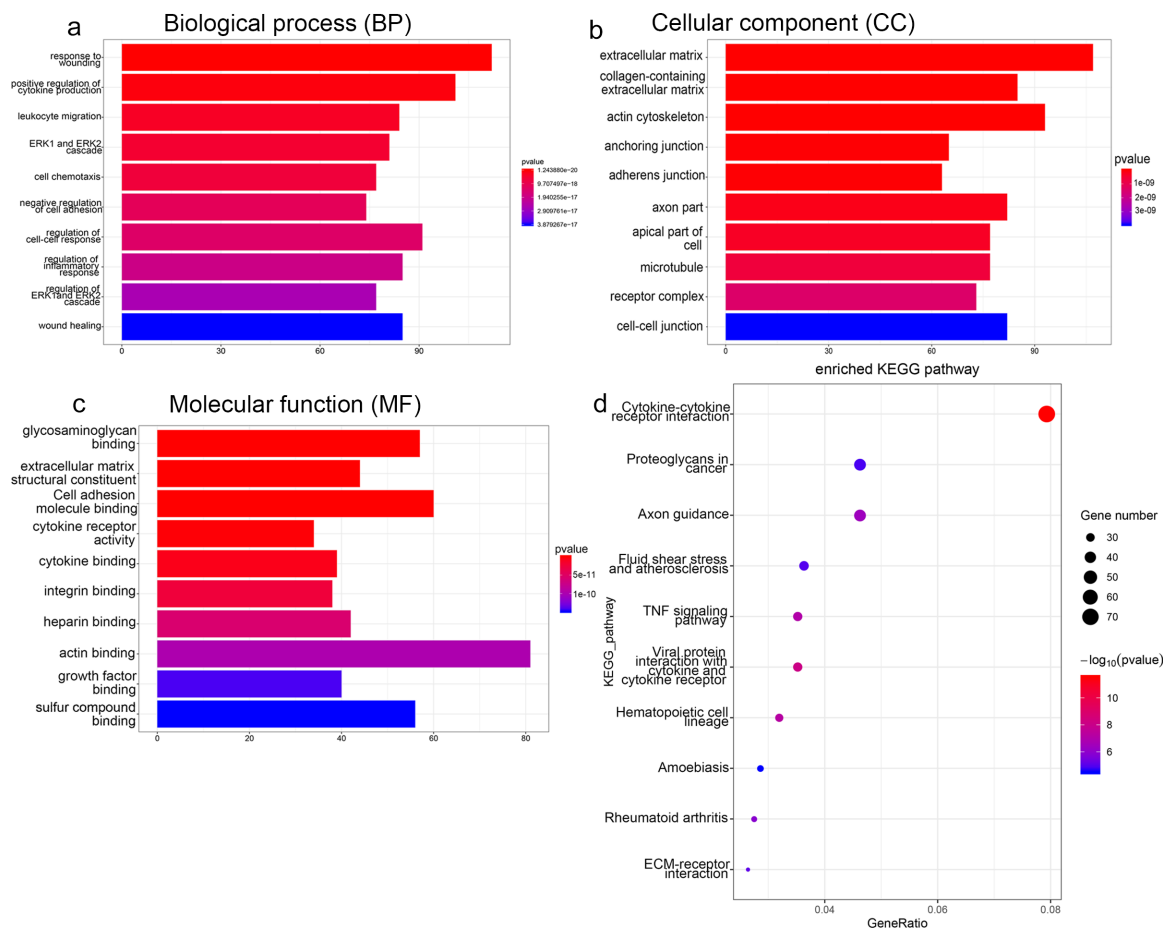


Figure 4. Functional annotation analyses of DEGs identified by sequencing RAW264.7 cells treated with RANKL or RANKL and UA. Gene ontology (GO) terms related to (a) biological process, (b) cellular components, and (c) molecular function are shown. (d) DEGs subject to the Kyoto Encyclopedia of Genes and Genomes (KEGG) pathway analysis are most enriched in signaling pathways related to stress, inflammation, differentiation, and disease.

RAW264.7 cells (negative control) than in the shBMP2-RAW264.7 cells ($P < 0.05$, Figure 6(a)), suggesting that stably transfected shBMP2-RAW264.7 cells were successfully established.

Bone biopsy specimens in the presence of shNC-RAW264.7 or shBMP2-RAW264.7 cells were treated with RANKL or RANKL + UA and imaged with scanning electron microscopy to investigate the effects of BMP2 on bone metabolism. In the RANKL-treated shNC cell group, the biopsy specimens showed many shallow, rough, and scattered bone resorption pits with varied sizes and clear boundaries (Figure 6(b)). In the RANKL + UA-treated shNC group, by contrast, few bone resorption pits in the specimens were visible. Remarkably, in the RANKL + UA-treated shBMP2 group, bone resorption pits were again more abundant. Quantitative analysis confirmed that the bone resorption area significantly decreased after UA

treatment compared with that after RANKL treatment only ($P < 0.05$), clearly increasing in the RANKL + UA-treated shBMP2 group, relative to that in the RANKL + UA-treated shNC group ($P < 0.05$, Figure 6(c)). These results indicate that UA attenuates osteoclast-driven bone resorption, whereas BMP2 silencing counteracts this effect.

Western blotting analysis

Protein expression levels of Akt1/P38/ERK pathway-related proteins and osteoclastic proteins (RANK, cathepsin K, and integrin $\beta 3$) were assessed by Western blotting in RANKL or RANKL + UA-treated cells. Representative Western blot images are summarized in Figure 7(a). No significant differences in the levels of p-Akt1/Akt1, p-P38/P38, p-ERK1/ERK1,

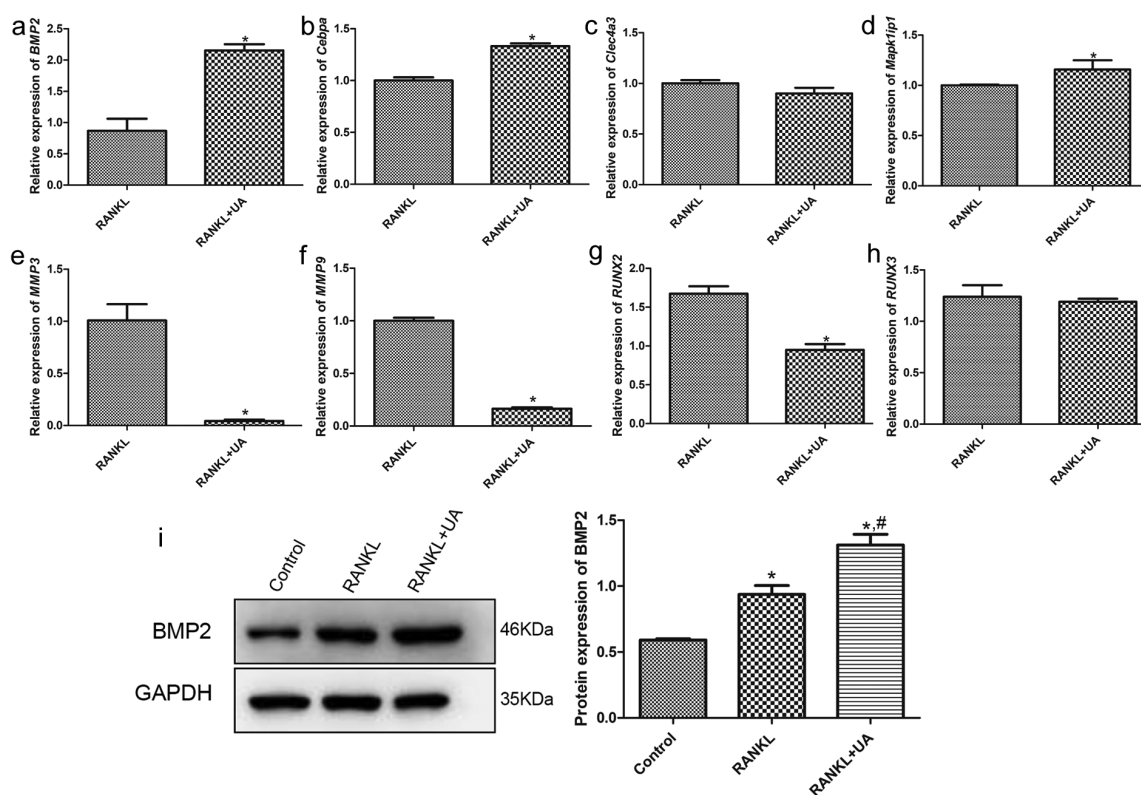


Figure 5. Verifying DEGs by reverse transcription-quantitative PCR. The relative mRNA expression of (a) *BMP2*, (b) *Cebpa*, (c) *Clec4a3*, (d) *Mapk1ip1*, (e) *MMP3*, (f) *MMP9*, (g) *RUNX2*, and (h) *RUNX3* in RANKL- or RANKL + UA-treated RAW264.7 cells. * $P < 0.05$ depicts significance compared with the RANKL-treated cell group. (i) The BMP2 protein expression detected by Western blotting. * $P < 0.05$ is significance compared with the control group; # $P < 0.05$, with the RANKL-treated group.

p-ERK2/ERK2, RANK, cathepsin K, or integrin β 3 between the control and RANKL + UA-treated shNC cell group were observed ($P > 0.05$, Figure 7). The levels of p-Akt1/Akt1 and p-P38/P38 were significantly higher in the RANKL- and RANKL + UA-treated sh*BMP2* group than in the control group ($P < 0.05$, Figure 7(b,c)). UA decreased the levels of RANKL-activated p-Akt1/Akt1 and p-p38/p38 ($P < 0.05$), but after *BMP2* knockdown, their levels rose again compared with those in the RANKL + UA-treated shNC group ($P < 0.05$, Figure 7(b,c)). In addition, the levels of p-ERK1/ERK1 and p-ERK2/ERK2 were similar to Akt1/p38 pathway-related protein levels across the groups (Figure 7(d,e)). The expression levels of RANK, cathepsin K, and integrin β 3 were significantly higher in the RANKL-treated group than in the control group ($P < 0.05$), and UA significantly decreased their RANKL-induced expression ($P < 0.05$, Figure 7(f-h)). When *BMP2* was silenced, it considerably increased the protein

levels in the RANKL + UA-treated shNC group ($P < 0.05$, Figure (f-h)).

Discussion

Osteoporosis is a systemic bone disease that increases the susceptibility to fracture and may be caused by excessive bone resorption due to increased osteoclast activity [25,26]. UA is a gut-microbial metabolite derived from pomegranate ellagitannins and has a protective effect against osteoarthritis development in vivo and in vitro [27,28]. Pomegranate peel extract prevents bone microarchitecture impairment and loss of bone mineral density in osteoarthritis. It also stimulates osteoblastic differentiation in vitro, alleviating osteoporosis[29]. Chen et al.[30] demonstrated that UA prevents brain aging caused by D-gal through the miR-34a-mediated activation of the SIRT1/mTOR signaling pathway, indicating its neuroprotective role. Therefore, we speculated

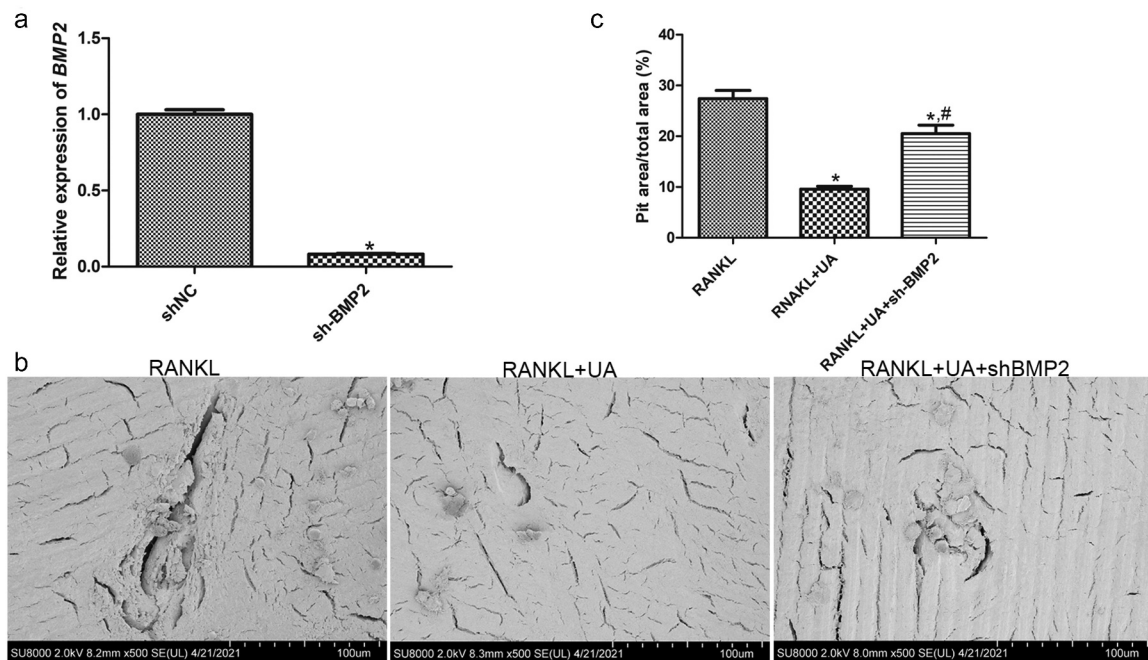


Figure 6. Effects of BMP2 on bone metabolism determined by gene silencing and scanning electron microscopy. (a) Cell transfection efficiency of shBMP2-RAW264.7 cells was assessed by quantifying *BMP2* expression with RT-qPCR. * $P < 0.05$ shows significance compared with shNC-RAW264.7 cells (negative control). (b) Representative scanning electron images of bone biopsy specimens on RANKL and UA treatments in the presence of shBMP2-RAW264.7 or shNC-RAW264.7 cells. (c) The bone biopsy area was quantified using the ImageJ software. * $P < 0.05$ represents significance compared with the RANKL-treated group; # $P < 0.05$, compared with the RANKL + UA-treated group.

that UA regulates osteoclast activity and the progression of osteoporosis. TRACP is a marker for bone resorption and osteoclast activity[31], which are important for understanding bone metabolism under physiological conditions and various pathological conditions[32]. Sekiguchi et al.[33] reported that mangiferin significantly reduces the formation of TRACP-positive multinuclear cells, which indicates that mangiferin inhibits osteoclast differentiation. *TRAP*, *NFATC1* and *c-Fos* are osteoclast-specific gene markers[34]. Our study showed that RANKL significantly increased TRACP and transcript levels of all three markers relative to those in the control cells. However, UA treatment reverted their RANKL-induced levels almost to those of control cells. Taken together, RANKL promotes differentiation of RAW264.7 cells into osteoclasts, whereas UA suppresses it.

Total RNA was isolated from cells subject to RANKL treatment or the combined treatment with UA and sequenced to understand how UA inhibits RANKL-driven osteoclast differentiation. The transcriptome dataset revealed 2,399 DEGs, of which 587 were induced and 1,812 repressed.

Among the notable activated genes were *BMP2*, *Cebpa*, and *Mapk1ip1*. *BMP2* is a potent growth factor that regulates osteoblast and osteoclast formation. Durbano et al.[35] indicated more significant differences in BMP signaling pathways in patients diagnosed with osteoporosis than in healthy control individuals. *Cebpa* is a key regulator of osteoclast lineage stereotyping, and its deficiency in osteoclasts can prevent bone loss[36]. Furthermore, *Mapk1ip1* expression is increased in osteosarcoma cells[37] but never assessed in osteoporosis. The repressed DEGs included *MMP3*, *MMP9*, and *RUNX2*. *MMP3* and *MMP9* are upregulated in chondrocytes in osteoarthritis [38]. Transcription factor *RUNX2* is critical for osteoblast differentiation and chondrocyte maturation and usually upregulated in chondrocytes in osteoarthritis[39]. Collectively, these differentially expressed genes, especially *BMP2*, may be involved in suppressing RANKL-induced osteoclast differentiation by UA.

Functional annotation analyses showed that the identified DEGs were associated with rheumatoid arthritis, the regulation of the ERK1/2 cascade,

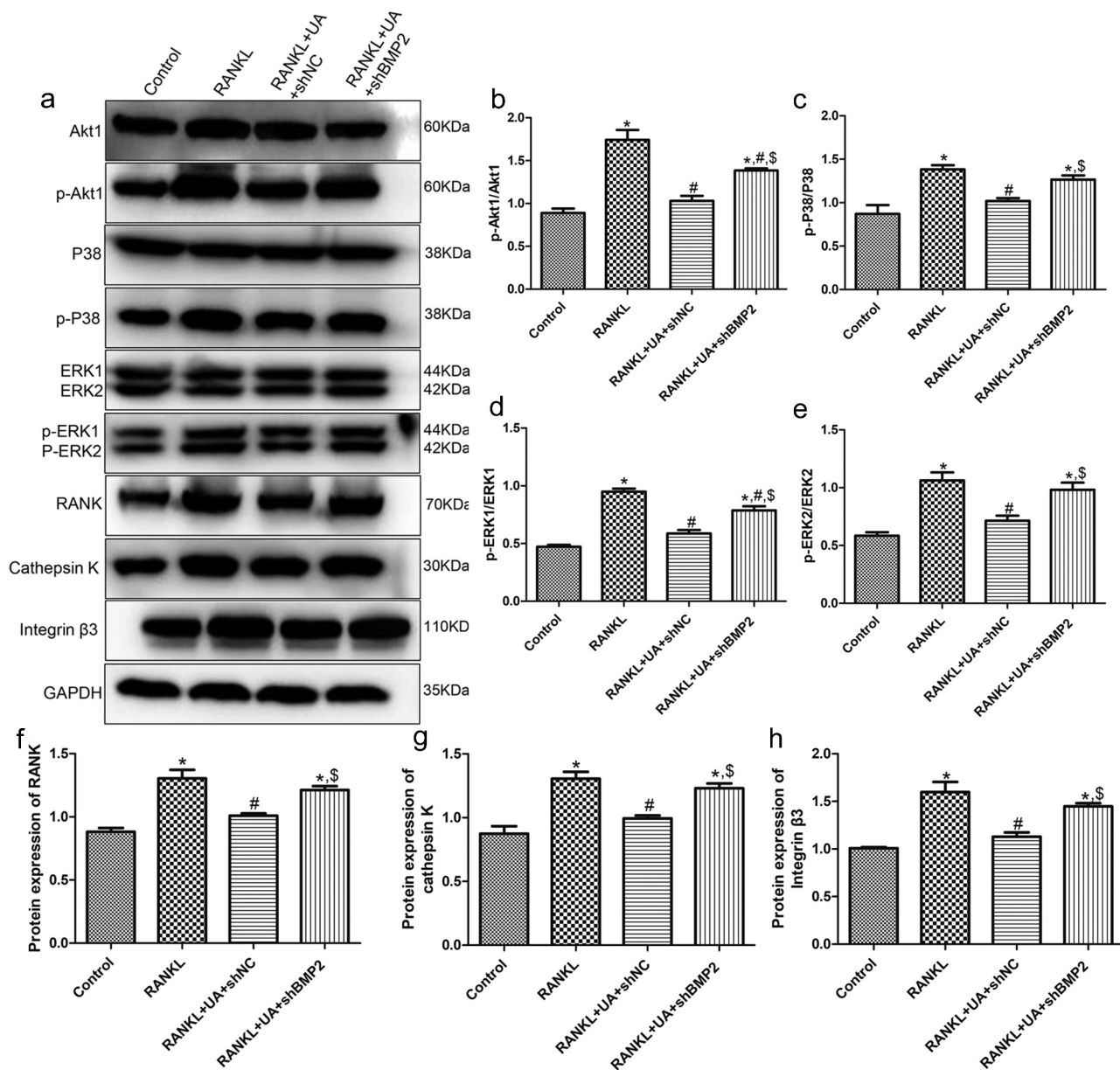


Figure 7. Protein expression levels of Akt1/p38/ERK pathway-related proteins and osteoclastic proteins RANK, cathepsin K, and integrin β 3 detected by Western blotting. (a) Representative Western blot images. The levels of (b) phosphorylated (p)-Akt1/Akt1, (c) p-P38/P38, (d) p-ERK1/ERK1, (e) p-ERK2/ERK2, (f) RANK, (g) cathepsin K, and (h) integrin β 3 are shown. * $P < 0.05$ shows significance compared with the untreated shNC group; # $P < 0.05$, with the RANKL-treated shNC group; $^{\$}P < 0.05$, with the RANKL + UA-treated shNC group.

ECM-receptor interactions, the regulation of inflammatory response, and the TNF signaling pathway. The ERK1/2 cascade, for example, regulates various processes, such as cell proliferation, differentiation, adhesion, migration, and cell cycle progression[40]. Activated T and B cells produce pro-osteoclastogenic factors, such as TNF- α , NF- κ B, RANKL, and IL-17A, accelerating bone loss in inflammatory states [15,41]. In the absence of estrogen, activated T cells secrete IL-17A,

RANKL, and TNF, enhancing bone resorption and causing postmenopausal osteoporosis[15]. Rheumatoid arthritis is an inflammatory disease that predisposes patients to osteoporosis[42]. Zhou et al. identified 3,179 DEGs in elderly patients with osteoporosis, non-osteoporotic elderly controls, and non-osteoporotic young donors. They found that these genes are enriched in ECM-receptor interactions, indicating they may be related to osteoporosis[43]. Furthermore, TNF-

α increases the expression of RANKL and sclerostin in osteocytes and promotes osteoclast formation[44]. These findings and our sequencing results imply that UA may relieve osteoclast differentiation by regulating multiple signaling pathways. However, their specific regulatory roles in the UA treatment of osteoporosis require further investigation.

BMP2 induces osteogenic differentiation in various cells. In mesenchymal stem cells, it causes chondrogenic differentiation and endochondral ossification. It is also essential for bone engineering[45]. Long non-coding RNA *MSC-AS1* promotes osteogenic differentiation by binding *miR-140-5p* to upregulate BMP2, relieving osteoporosis [46]. In addition, high BMP2 expression enhances osteoclast-mediated bone resorption through the classical BMP signaling pathway and p65 signaling pathway[47]. These findings suggest the importance of BMP2 in osteoclasts and osteoporosis. In our study, BMP2 expression was considerably higher in the RANKL + UA-treated RAW264.7 cells than in the RANKL-treated. Thus, BMP2 was selected as a candidate for further investigation. RANKL-treated RAW264.7 cells formed bone resorption pits in bone biopsy specimens, but UA inhibited their formation. Remarkably, BMP2 knockdown restored bone resorption. Taken together, UA suppresses osteoclast differentiation and bone resorption by regulating BMP2 expression.

Akt1 is an overactive proto-oncogene in most cancers[48]. It is also a crucial promoter of osteoblast-osteoclast coupling[49]. Activated p38 phosphorylates osteoblast- or osteoclast-related transcription factors and triggers other pathways by activating cytoplasmic substrates, such as Akt and pMK2[50]. ERK1 and ERK2, both expressed in osteoblasts, have essential roles in the Ras-RAF-MEK-ERK signal transduction cascade[51]. This cascade regulates multiple processes, including cell cycle progression, differentiation, osteoclastogenesis, metabolism, and transcription[52]. Fowler et al.[53] demonstrated that activin A completely inhibits RANKL-stimulated osteoclast differentiation, migration, and bone resorption via SMAD2, Akt1, and I κ B signaling. Another study reported that *Rev-erba* negatively mediates osteoblast and osteoclast differentiation by suppressing the p38

MAPK pathway[54]. Furthermore, Yue et al.[55] showed that prostaglandin D₂ promotes osteoclast apoptosis through the ERK1/2 and Akt signaling pathways. We conclude that UA represses the RANKL-induced osteoclast differentiation of RAW264.7 cells by regulating Akt1, p38, and ERK1/2 signaling pathways, and that BMP2 may reverse the UA inhibitory effect via these pathways.

RANKL/RANK signaling activates a central regulator of osteoclast generation NFATc1, inducing osteoclast gene expression[56]. Cathepsin K is highly expressed in osteoclasts, and its inhibitors have been developed for osteoporosis management [57]. Integrin β 3 regulates cell adhesion and contributes to differentiation, promoting bone formation[58]. Zeng et al.[59] found that aconine decreases the levels of the osteoclast-specific genes integrin β 3 and cathepsin K, repressing RANKL-induced osteoclast differentiation. Therefore, UA treatment may inhibit RANKL-induced osteoclast formation by downregulating RANK, cathepsin K, and integrin β 3, whereas BMP2 may reverse this effect.

Conclusions

We identified 2,399 differentially expressed genes in UA-promoted inhibition of osteoclast differentiation. UA may suppress the RANKL-induced osteoclast differentiation by regulating Akt1, p38, and ERK1/2 signaling pathways and repressing osteoclast-related proteins. Additionally, BMP2 was shown to be a novel UA target in inhibiting osteoclast differentiation. However, the regulatory roles of the identified genes, except *BMP2*, and the signaling pathways require further investigation. The potential therapeutic effects of UA on osteolytic diseases require further confirmation by culturing osteoblasts with conditioned medium from osteoclast cultures and in vivo experiments. Our results uncover the role of UA in regulating osteoclast activity and provide insights into the underlying mechanisms. Moreover, our findings propose BMP2 as a potential drug target for the therapy of bone metabolic diseases, such as osteoporosis, based on its roles in osteoclast differentiation.

Highlights

- UA inhibition of osteoclast differentiation involves 2,399 DEGs.
- UA suppresses RANKL-induced osteoclast differentiation via Akt1, p38, and ERK1/2.
- BMP2 is a novel UA target for inhibiting osteoclast differentiation.

Disclosure statement

No potential conflict of interest was reported by the author(s).

Funding

This work was supported by the Featured Clinical Discipline Project of Shanghai Pudong New District (PWYts2018-2), the Construction of Key Discipline Group of Sanitary System of Shanghai Pudong New District (PWZxq2017-12), the Shanghai Pudong Science and Technology Development Funding (PKJ2020-Y44), and Shanghai Sailing Program (21YF1405800), and Promotion Project of Advanced and Appropriate Technology from Shanghai Healthcare Commission (2019SY069).

Data availability

The dataset used and/or analyzed during the current study are available from the corresponding author on reasonable request.

Author contributions

Zhe Wang, Guobin Qi, and Xiuhui Wang designed the experiments; Zhe Wang, Guobin Qi, Zhuokai Li, Xu Cui, Shengyang Guo, Yueqi Zhang, and Pan Cai performed the experiments and analyzed the experimental results; Zhe Wang and Xiuhui Wang obtained the funding and supervised the experiment; Zhe Wang and Guobin Qi drafted the paper, and Xiuhui Wang revised. All authors have reviewed and approved the submitted version of the manuscript.

References

- [1] Song C, Yang X, Lei Y, et al. Evaluation of efficacy on RANKL induced osteoclast from RAW264.7 cells. *J Cell Physiol*. 2019;234(7):11969–11975.
- [2] Kim JM, Lin C, Stavre Z, et al. Osteoblast-osteoclast communication and bone homeostasis. *Cells*. 2020;9(9):2073.
- [3] Boyle WJ, Simonet WS, Lacey DL. Osteoclast differentiation and activation. *Nature*. 2003;423(6937):337–342.
- [4] Gosch M, Kammerlander C, Nicholas JA. Treatment of osteoporosis in older adults. *Panminerva Med*. 2014;56(2):133–143.
- [5] Yun H, Delzell E, Saag KG, et al. Fractures and mortality in relation to different osteoporosis treatments. *Clin Exp Rheumatol*. 2015;33(3):302–309.
- [6] Shao H, Wu R, Cao L, et al. Trelagliptin stimulates osteoblastic differentiation by increasing runt-related transcription factor 2 (RUNX2): a therapeutic implication in osteoporosis. *Bioengineered*. 2021;12(1):960–968.
- [7] Noh JY, Yang Y, Jung H. Molecular mechanisms and emerging therapeutics for osteoporosis. *Int J Mol Sci*. 2020;21(20):7623.
- [8] Saha P, Yeoh BS, Singh R, et al. Gut microbiota conversion of dietary ellagic acid into bioactive phytochemical urolithin A inhibits heme peroxidases. *PLoS One*. 2016;11(6):e0156811.
- [9] Norden E, Heiss EH. Urolithin A gains in antiproliferative capacity by reducing the glycolytic potential via the p53/TIGAR axis in colon cancer cells. *Carcinogenesis*. 2019;40(1):93–101.
- [10] Andreux PA, Blanco-Bose W, Ryu D, et al. The mitophagy activator urolithin A is safe and induces a molecular signature of improved mitochondrial and cellular health in humans. *Nat Metab*. 2019;1(6):595–603.
- [11] Ding SL, Pang ZY, Chen XM, et al. Urolithin A attenuates IL-1beta-induced inflammatory responses and cartilage degradation via inhibiting the MAPK/NF-kappaB signaling pathways in rat articular chondrocytes. *J Inflamm (Lond)*. 2020;17(1):13.
- [12] Lin J, Zhuge J, Zheng X, et al. Urolithin A-induced mitophagy suppresses apoptosis and attenuates intervertebral disc degeneration via the AMPK signaling pathway. *Free Radic Biol Med*. 2020;150:109–119.
- [13] Kukita T, Wada N, Kukita A, et al. RANKL-induced DC-STAMP is essential for osteoclastogenesis. *J Exp Med*. 2004;200(7):941–946.
- [14] Liou YM, Chan CL, Huang R, et al. Effect of l-caldesmon on osteoclastogenesis in RANKL-induced RAW264.7 cells. *J Cell Physiol*. 2018;233(9):6888–6901.
- [15] Weitzmann MN. Bone and the Immune System. *Toxicol Pathol*. 2017;45(7):911–924.
- [16] Chen X, Zhu G, Jin T, et al. Cadmium induces differentiation of RAW264.7 cells into osteoclasts in the presence of RANKL. *Food Chem Toxicol*. 2011;49(9):2392–2397.
- [17] Zamani M, Zamani V, Heidari B, et al. Prevalence of osteoporosis with the World Health Organization diagnostic criteria in the Eastern mediterranean region: a systematic review and meta-analysis. *Arch Osteoporos*. 2018;13(1):129.
- [18] Tian Y, Gong Z, Zhao R, et al. Melatonin inhibits RANKL-induced osteoclastogenesis through the miR882/Reverbalpha axis in Raw264.7 cells. *Int J Mol Med*. 2021;47(2):633–642.

- [19] Fujimoto M, Mano Y, Anai M, et al. Epigenetic alteration to activate Bmp2-Smad signaling in Raf-induced senescence. *World J Biol Chem.* 2016;7(1):188–205.
- [20] Qiao H, Wang YF, Yuan WZ, et al. Silencing of ENO1 by shRNA inhibits the proliferation of gastric cancer cells. *Technol Cancer Res Treat.* 2018;17:1533033818784411.
- [21] Qiu N, Zhou H, Xiao Z. Downregulation of PKD1 by shRNA results in defective osteogenic differentiation via cAMP/PKA pathway in human MG-63 cells. *J Cell Biochem.* 2012;113(3):967–976.
- [22] Fu Y, Hu X, Gao Y, et al. LncRNA ROR/miR-145-5p axis modulates the osteoblasts proliferation and apoptosis in osteoporosis. *Bioengineered.* 2021;12(1):7714–7723.
- [23] Deng Y, Tong J, Shi W, et al. Thromboangiitis obliterans plasma-derived exosomal miR-223-5p inhibits cell viability and promotes cell apoptosis of human vascular smooth muscle cells by targeting VCAM1. *Ann Med.* 2021;53(1):1129–1141.
- [24] Yang H, Zhou J, Wang J, et al. Circulating exosomal MicroRNA profiles associated with acute soft tissue injury. *Cell J.* 2021;23(4):474–484.
- [25] Mei L, Li M, Zhang T. MicroRNA miR-874-3p inhibits osteoporosis by targeting leptin (LEP). *Bioengineered.* 2021;12(2):11756–11767.
- [26] Khosla S, Hofbauer LC. Osteoporosis treatment: recent developments and ongoing challenges. *Lancet Diabetes Endocrinol.* 2017;5(11):898–907.
- [27] Fu X, Gong LF, Wu YF, et al. Urolithin A targets the PI3K/Akt/NF- κ B pathways and prevents IL-1 β -induced inflammatory response in human osteoarthritis: in vitro and in vivo studies. *Food Funct.* 2019;10(9):6135–6146.
- [28] Spilmont M, Leotoing L, Davicco MJ, et al. Pomegranate peel extract prevents bone loss in a preclinical model of osteoporosis and stimulates osteoblastic differentiation in vitro. *Nutrients.* 2015;7(11):9265–9284.
- [29] Hartman RE, Shah A, Fagan AM, et al. Pomegranate juice decreases amyloid load and improves behavior in a mouse model of Alzheimer's disease. *Neurobiol Dis.* 2006;24(3):506–515.
- [30] Chen P, Chen F, Lei J, et al. Activation of the miR-34a-mediated SIRT1/mTOR signaling pathway by urolithin A attenuates D-galactose-induced brain aging in mice. *Neurotherapeutics.* 2019;16(4):1269–1282.
- [31] Lin Z, Huang S, and LingHu X, et al. Perillaldehyde inhibits bone metastasis and receptor activator of nuclear factor-kappaB ligand (RANKL) signaling-induced osteoclastogenesis in prostate cancer cell lines. *Bioengineered.* 2021;133 2710–2719.
- [32] Solberg LB, Brorson SH, Stordalen GA, et al. Increased tartrate-resistant acid phosphatase expression in osteoblasts and osteocytes in experimental osteoporosis in rats. *Calcif Tissue Int.* 2014;94(5):510–521.
- [33] Sekiguchi Y, Mano H, Nakatani S, et al. Mangiferin positively regulates osteoblast differentiation and suppresses osteoclast differentiation. *Mol Med Rep.* 2017;16(2):1328–1332.
- [34] Chen H, Li S, Yin H, et al. MYC-mediated miR-320a affects receptor activator of nuclear factor kappaB ligand (RANKL)-induced osteoclast formation by regulating phosphatase and tensin homolog (PTEN). *Bioengineered.* 2021;12(2):12677–12687.
- [35] Durbano HW, Halloran D, Nguyen J, et al. Aberrant BMP2 Signaling in Patients Diagnosed with Osteoporosis. *Int J Mol Sci.* 2020;21(18):6909.
- [36] Chen W, Zhu G, Tang J, et al. C/ebpalpha controls osteoclast terminal differentiation, activation, function, and postnatal bone homeostasis through direct regulation of Nfatc1. *J Pathol.* 2018;244(3):271–282.
- [37] Fu D, Liu S, Liu J, et al. iTRAQ-based proteomic analysis of the molecular mechanisms and downstream effects of fatty acid synthase in osteosarcoma cells. *J Clin Lab Anal.* 2021;35(3):e23653.
- [38] Kim JH, Jeon J, Shin M, et al. Regulation of the catabolic cascade in osteoarthritis by the zinc-ZIP8-MTF1 axis. *Cell.* 2014;156(4):730–743.
- [39] Komori T. Runx2, an inducer of osteoblast and chondrocyte differentiation. *Histochem Cell Biol.* 2018;149(4):313–323.
- [40] Roskoski R Jr. ERK1/2 MAP kinases: structure, function, and regulation. *Pharmacol Res.* 2012;66(2):105–143.
- [41] Pietschmann P, Mechtcheriakova D, Meshcheryakova A, et al. Immunology of osteoporosis: a mini-review. *Gerontology.* 2016;62(2):128–137.
- [42] Adami G, Saag KG. Osteoporosis pathophysiology, epidemiology, and screening in rheumatoid arthritis. *Curr Rheumatol Rep.* 2019;21(7):34.
- [43] Zhou Z, Gao M, Liu Q, et al. Comprehensive transcriptome analysis of mesenchymal stem cells in elderly patients with osteoporosis. *Aging Clin Exp Res.* 2015;27(5):595–601.
- [44] Kitaura H, Marahleh A, Ohori F, et al. Osteocyte-related cytokines regulate osteoclast formation and bone resorption. *Int J Mol Sci.* 2020;21(14):5169.
- [45] Zhou N, Li Q, Lin X, et al. BMP2 induces chondrogenic differentiation, osteogenic differentiation and endochondral ossification in stem cells. *Cell Tissue Res.* 2016;366(1):101–111.
- [46] Zhang N, Hu X, He S, et al. LncRNA MSC-AS1 promotes osteogenic differentiation and alleviates osteoporosis through sponging microRNA-140-5p to upregulate BMP2. *Biochem Biophys Res Commun.* 2019;519(4):790–796.
- [47] Miao X, Yuan J, Wu J, et al. Bone morphogenetic protein-2 promotes osteoclasts-mediated osteolysis via Smad1 and p65 signaling pathways. *Spine (Phila Pa 1976).* 2021;46(4):E234–E42.
- [48] Balasuriya N, McKenna M, Liu X, et al. Phosphorylation-dependent inhibition of Akt1. *Genes (Basel).* 2018;9(9):450.
- [49] Mukherjee A, Rotwein P. Selective signaling by Akt1 controls osteoblast differentiation and osteoblast-mediated osteoclast development. *Mol Cell Biol.* 2012;32(2):490–500.

- [50] Rodriguez-Carballo E, Gamez B, Ventura F. p38 MAPK signaling in osteoblast differentiation. *Front Cell Dev Biol.* [2016](#);4:40.
- [51] Koga Y, Tsurumaki H, Aoki-Saito H, et al. Roles of cyclic AMP response element binding activation in the ERK1/2 and p38 MAPK signalling pathway in central nervous system, cardiovascular system, osteoclast differentiation and mucin and cytokine production. *Int J Mol Sci.* [2019](#);20(6):1346.
- [52] Matsushita T, Chan YY, Kawanami A, et al. Extracellular signal-regulated kinase 1 (ERK1) and ERK2 play essential roles in osteoblast differentiation and in supporting osteoclastogenesis. *Mol Cell Biol.* [2009](#);29(21):5843–5857.
- [53] Fowler TW, Kamalakar A, Akel NS, et al. Activin A inhibits RANKL-mediated osteoclast formation, movement and function in murine bone marrow macrophage cultures. *J Cell Sci.* [2015](#);128(4):683–694.
- [54] Kim K, Kim JH, Kim I, et al. Rev-erbalph α negatively regulates osteoclast and osteoblast differentiation through p38 MAPK signaling pathway. *Mol Cells.* [2020](#);43(1):34–47.
- [55] Yue L, Haroun S, Parent JL, et al. Prostaglandin D(2) induces apoptosis of human osteoclasts through ERK1/2 and Akt signaling pathways. *Bone.* [2014](#);60:112–121.
- [56] Ono T, Nakashima T. Recent advances in osteoclast biology. *Histochem Cell Biol.* [2018](#);149(4):325–341.
- [57] Drake MT, Clarke BL, Oursler MJ, et al. Cathepsin K inhibitors for osteoporosis: biology, potential clinical utility, and lessons learned. *Endocr Rev.* [2017](#);38(4):325–350.
- [58] Lopes HB, Freitas GP, Elias CN, et al. Participation of integrin beta3 in osteoblast differentiation induced by titanium with nano or microtopography. *J Biomed Mater Res A.* [2019](#);107(6):1303–1313.
- [59] Zeng XZ, He LG, Wang S, et al. Aconine inhibits RANKL-induced osteoclast differentiation in RAW264.7 cells by suppressing NF-kappaB and NFATc1 activation and DC-STAMP expression. *Acta Pharmacol Sin.* [2016](#);37(2):255–263.